Comparison of GPS analysis strategies for high-accuracy vertical land motion

Article *in* Physics and Chemistry of the Earth Parts A/B/C · January 2008

DOI: 10.1016/j.pce.2006.11.003

Available online at www.sciencedirect.com
ScienceDirect
Physics and Chemistry of the Earth 33 (2008) 194–204
PHYSICS and CHEMISTRY of the EARTH
www.elsevier.com/locate/pce

Comparison of GPS analysis strategies for high-accuracy vertical land motion

Halfdan P. Kierulf [a,*], Hans-Peter Plag [g,a], Richard M. Bingley [b], Norman Teferle [b], Coskun Demir [c], Ayhan Cingoz [c], Hasan Yildiz [c], Jorge Garate [d], Jose M. Davila [d], Cristina G. Silva [d], Ryszard Zdunek [e], Leszek Jaworski [e], Juan J. Martinez-Benjamin [f], Raul Orus [f], Angela Aragon [f]

[a] *Norwegian Mapping Authority, Kartverksveien 21, N-3511 Hønefoss, Norway*
[b] *Institute of Engineering Surveying and Space Geodesy, University of Nottingham, UK*
[c] *General Command of Mapping, Ankara, Turkey*
[d] *Real Instituto y Observatorio de la Armada, Cadiz, Spain*
[e] *SRC Space Research Centre, Polish Academy of Science, Warsawa, Poland*
[f] *Universidad Politecnica de Cataluna, Barcelona, Spain*
[g] *Nevada Bureau of Mines and Geology and Seismological Laboratory, University of Nevada, Reno, USA*

Accepted 18 November 2006
Available online 3 May 2007

Abstract

Tide gauges measure sea level changes relative to land. To separate absolute changes in sea level from vertical land movements tide gauges are often co-located with Continuous GPS (CGPS). In order to achieve an accuracy of better than 1 mm/yr, as required for sea level studies in the global change context, vertical land motion needs to be determined with the same accuracy. This is an ambitious goal for CGPS and needs a carefully designed analysis strategy. We have compared the independent results from six different analysis centres, using three different GPS processing softwares and a number of different analysis strategies.

Based on the comparison, we discuss the achieved accuracy and the quality of the different strategies. The data analysed are from the CGPS network of the European Sea Level Service and cover the time window from the beginning of 2000 until the end of 2003. The comparison reveals large differences in the day-to-day variations of the coordinate time series and also in the seasonal cycle contained in these. The trends show systematic differences, depending on software and strategy used. To a large extent, the latter deviations can be explained by differences in the realisation of the reference frame, while some parts may be due to other, as yet, unidentified contributions. The results suggest that the reference frame and its relation to the center of mass of the Earth system may be the main limitation in achieving the accuracy goal for the secular velocity of vertical land motion.

Keywords: Continuous GPS; Vertical land movements; Tide gauge monitoring; GPS analysis strategy

1. Introduction

For studies of global change, sea level is a crucial parameter. Relative sea level has been observed by tide gauges at many coastal locations, at some for up to two hundred years. These tide gauges measure sea level relative to benchmarks on land. Satellite altimetry has contributed sea level observations over more than a decade with near global coverage in a geocentric coordinate system. In order to derive absolute sea level changes from tide gauges, the observations need to be corrected for vertical motion of the benchmark (i.e. the land). Therefore, an increasing number of tide gauges are collocated with Continuous GPS (CGPS). Currently, co-location with CGPS is the only

* Corresponding author.
E-mail address: halfdan.kierulf@statkart.no (H.P. Kierulf).

1474-7065/$ - see front matter © 2007 Elsevier Ltd. All rights reserved.
doi:10.1016/j.pce.2006.11.003

practically available technique to get high-accuracy determinations of land motion in a global, geocentric reference frame with a globally homogeneous accuracy. Moreover, the comparison of tide gauge records to satellite altimetry observations requires to position the tide gauges in the same geocentric coordinate system as the altimeter. Providing ground-truth for the satellite altimeter is, therefore, also achieved by having the tide gauges co-located with CGPS. Global and regional sea level studies in the context of climate and global change require an accuracy of better than 1 mm/yr (Church et al., 2001). Consequently, the vertical velocities at the CGPS stations also need to be determined with an accuracy with respect to a stable, global, geocentric reference frame better than 1 mm/yr (Bevis et al., 2000).

The determination of secular vertical velocities with an accuracy of better than 1 mm/yr in a global reference frame is a rather demanding task depending not only on the analysis of the GPS observations but also equipment used, station conditions, stability of the operational environment, length of the records, and, finally the stability of the reference frame itself. In order to mitigate the contribution from the GPS analysis to the error budget of the vertical trends, a number of international projects have been established. An example is the *GPS Tide Gauge Benchmark Monitoring Pilot Project* (TIGA-PP, see http://129.247.162.38/tiga/index_TIGA.html) of the *International GNSS Service* (IGS), which attempts, through a re-analysis of the observations from the global IGS network, to determine a highly stable global reference frame for the vertical land motion at the tide gauges. Another example is provided by *European Sea Level Service* (ESEAS), which developed a GPS analysis strategy, taking into account that the network of CGPS stations co-located with tide gauges is rapidly expanding and thus not appropriate as a reference network. The ESEAS strategy therefore focuses on a separation of the determination of the global reference frame on the basis of a global stable reference network from the analysis of the CGPS data from stations co-located with tide gauges (Kierulf et al., 2004).

In order to assess the contribution of the GPS analysis itself to the error budget of coordinate time series and secular trends, we have compared the results from six ESEAS GPS Analysis Centres (AC). These results are obtained with three different analysis strategies and three different software packages. Moreover, three different sets of global products, i.e. Satellite Orbits and Clocks (SOC), are used. The observations are for the CGPS network of the ESEAS and cover a window of 4 years, which allows the determination of secular trends not contaminated by annual and semi-annual harmonic variations (Blewitt and Lavallée, 2002).

2. Data set

The CGPS observations are taken from the ESEAS CGPS Data archive at http://www.eseas.org/products/cgps/. Currently, the archive holds data for more than 30 CGPS stations at tide gauges in Europe. The locations of the CGPS stations are given in Fig. 1 and information on the available equipment is provided in Table 1. The station network represented by the data available in the ESEAS archive is heterogenous in terms of receivers, antennas, monumentation and station environments.

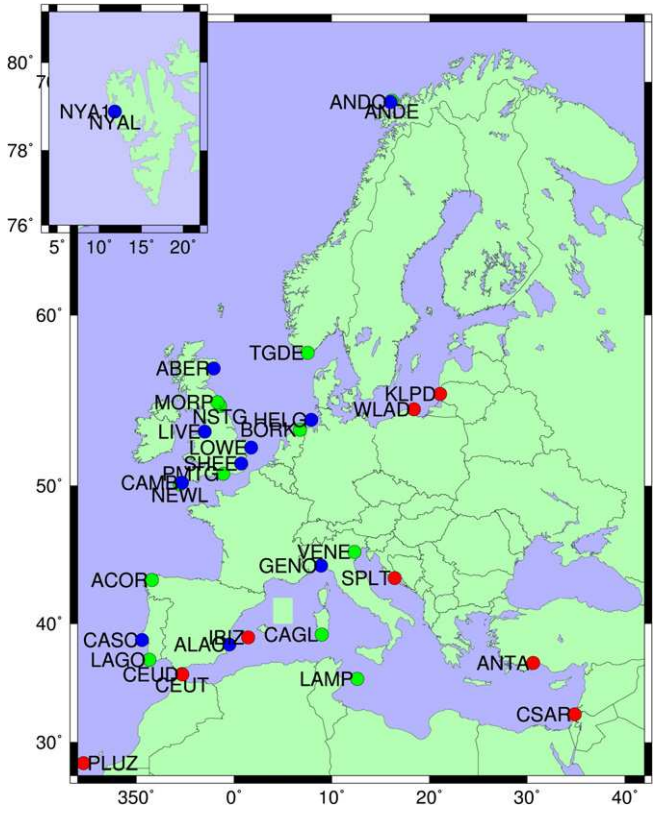

Fig. 1. ESEAS CGPS network. Blue dots are for high-quality stations included in the discussion in this paper, red dots are for ESEAS-RI stations founded by EU, not analysed by the ACs, and green dots are for the remaining stations in the ESEAS CGPS network, analysed by the ACs, but excluded from the discussion. (For interpretation of the references to colour in this figure legend, the reader is referred to the web version of this article.)

The interval selected for the inter-comparison covers the time window from the beginning of 2000 to the end of 2003. Twenty five of the CGPS stations shown in Fig. 1 cover most or all of this time window, and these stations are used in this study. Some of these records contain gaps, but in total approximately 30,000 station-days have been analysed, which is equivalent to the total amount of gaps being <18%.

3. CGPS analysis and coordinate time series analysis

The analysis of the GPS observations was carried out by six ESEAS AC using three different software packages, two different strategies for the determination of the reference frame, and three different SOCs. In total, nine different solutions were produced (Table 2).

Table 1
The ESEAS CGPS stations

STAT	Latitude	Longitude	Height receiver		Antenna	From	Source
ABER[c]	57.1440	−2.0802	53.47	ASH Z-XII3	ASH700936F_C S	2000.0	BIGF
ACOR	43.3643	−8.3989	69.99	ASH UZ-12	ASH700936D_M S	2000.0	EUREF
ALAC[c]	38.3389	−0.4812	60.33	TRM 4000SSI	TRM29659.00	2000.0	EUREF
ANDE	69.3260	16.1348	44.22	ROGUE SNR-8000	AOAD/M_T	2001.1	NMA
ANDO[c]	69.2783	16.0086	413.77	AOA BM ACT	AOAD/M_T	2000.0	NMA
ANTA[b]	36.8285	30.6094	33.28	ASH UZ-12	ASH701945E_M S	2003.9	ESEAS
BORK	53.5636	6.7474	54.22	TRM 4700	TRM29659.00 S[a]	2000.1	EUREF
CAGL	39.1359	8.9727	238.36	TRM 4700[a]	TRM29659.00	2000.0	IGS
CAMB[c]	50.2184	−5.3273	139.58	ASH UZ-12	ASH700936D_M S	2000.0	BIGF
CASC[c]	38.6934	−9.4185	77.13	LEICA RS500[a]	LEIAT504	2000.0	EUREF
CEUT	35.8960	−5.3113	51.86	TRM 4000SSI	TRM29659.00 S	2001.9	EUREF
CSAR[b]	32.4882	34.8901	36.67	TRM 5700	TRM29659.00	2004.3	ESEAS
GENO[c]	44.4193	8.9211	155.51	TRM 4000SSI	TRM29659.00	2000.0	IGS
HELG[c]	54.1744	7.8930	48.54	ASH Z-XII3	ASH700936D_M S	2000.0	EUREF
IBIZ[b]	38.9112	1.4489	59.50	JPS E_GGD	TPSCR3_GGD	2004.8	ESEAS
KLPD[b]	55.7153	21.1188	43.74	ASH Z-XII3	ASH700936E	2004.7	ESEAS
LAGO	37.0989	−8.6683	62.73	LEICA RS500[a]	LEIAT504	2000.3	EUREF
LAMP	35.4997	12.6056	57.87	TRM 4700[a]	TRM29659.00	2000.0	EUREF
LIVE[c]	53.4496	−3.0182	66.12	ASH Z-XII3	ASH700936F_C S	2000.0	BIGF
LOWE[c]	52.4732	1.7501	53.93	ASH Z-XII3	ASH700936F_C S	2000.0	BIGF
MORP	55.2127	−1.6854	144.44	ASH Z-XII3	AOAD/M_T	2000.2	BIGF
NEWL[c]	50.1030	−5.5427	64.51	ASH Z-XII3	ASH700936D_M S	2000.0	BIGF
NSTG	55.0074	−1.4398	56.91	ASH Z-XII3	ASH700936B_M S	2000.1	BIGF
NYA1[c]	78.9295	11.8653	84.20	AOA BM ACT	ASH701073.1 S	2000.0	IGS
NYAL[c]	78.9295	11.8650	78.47	AOA BM ACT	AOAD/M_B	2000.0	IGS
PLUZ[b]	28.1467	344.5923	50.35	TRM 5700	TRM29659.00	2004.3	ESEAS
PMTG	50.8023	−1.1112	56.54	ASH UZ-12	ASH701945C_M S	2001.7	BIGF
SHEE[c]	51.4456	0.7434	53.29	TRM 4000SSI	TRM29659.00	2000.0	BIGF
SPLT[b]	43.5066	16.4384	48.29	ASH UZ-12	ASH701945E_M S	2004.3	ESEAS
TGDE	58.0063	7.5547	45.83	AOA SNR-12 ACT	AOAD/M_T	2002.3	NMA
VENE	45.4369	12.3319	67.19	TRM 4700[a]	TRM29659.00	2000.0	IGS
WLAD[b]	54.7967	18.4187	34.74	ASH UZ-12	ASH701945E_M S	2003.3	ESEAS

BIGF: The British Isles GPS archiving Facility, EUREF: European Reference Frame, NMA: Norwegian Mapping Authority, ASH: Ashtech, TRM: Trimble, BM: Benchmark, S: Snow.

[a] Equipment shift during the period.

[b] Not included in the analysis of the ACs.

[c] High-quality records used in the comparison.

Three ACs used the GIPSY-OASIS II in the Precise Point Positioning (PPP) mode (Zumberge et al., 1997) with the precise SOCs provided by the *Jet Propulsion Laboratory* (JPL). In addition, two of these ACs also utilised the precise SOCs provided by the *International GPS Service* (IGS). The Bernese GPS software (Hugentobler et al., 2001, Version 4.2) was used by two ACs, one applying the Double Difference (DD) mode and using IGS precise SOCs, and the other applying the PPP mode using both IGS precise SOCs and IGS rapid (denoted here as IGR) SOCs. GAMIT/GLOBK (denoted here as GAMIT) (King and Bock, 2003; Herring, 2003) is used by one AC in the DD mode with IGS precise orbits.

The use of PPP within Bernese is only recommended for the computation of apriori coordinates for the Bernese-DD mode (Hugentobler et al., 2001), and therefore, its use for such an high accuracy application is not straight forward. The few references known to the authors mentioning Bernese in PPP mode simply used the software to evaluate IGS combined products over several weeks (Kouba and Springer, 2001; Kouba, 2003). Therefore, this approach by UNOTT to analysing the ESEAS CGPS network can be regarded as previously un-attempted in the geodetic community.

Using IGS precise SOCs for PPP results in a specific frame denoted here as IGS-P00, which is different from IGb00 with respect to scale and origin (Ray et al., 2004). This is a consequence of the minimum constraint solutions on which the IGS SOCs are based (Kouba and Springer, 2001). The origin of IGS-P00 follows the geocenter as sensed by GPS alone. Consequently, all trends in IGS-P00 are different from trends in ITRF2000. The IGR SOCs are given in IGb00, which is closely aligned to ITRF2000. Therefore, UNOTT also used the IGR SOC in the PPP analyses.

The ACs produced daily results for the 25 CGPS stations. The results are provided as time series of station displacements in north, east, and height, given with respect to mean station coordinates. For each station and each component, the analyses in principle result in nine time series. However, some of the ACs do not process all stations. The available solutions form the basis for the comparison

Table 2
The ESEAS CGPS analysis strategy

AC	P	S	GP	CM	γ	GM	OL	AMF
NMA	GIPSY	PPP	JPL	w.n.	10	C	HGS	Niell
NMA	GIPSY	PPP	IGS	w.n.	10	C	HGS	Niell
ROA	GIPSY	PPP	JPL	w.n.	10	C	HGS	Niell
UPC	GIPSY	PPP	JPL	w.n.	7	C	no	Niell
UPC	GIPSY	PPP	IGS	w.n.	7	C	no	Niell
UNOTT	Bern 4.2	PPP	IGS	w.n.	10	C	HGS	Niell
UNOTT	Bern 4.2	PPP	IGR	w.n.	10	C	HGS	Niell
SRC	Bern 4.2	RNS-DD	IGS	w.n.	10	C	HGS	Niell
GCM	GAMIT	RNS-DD	IGS	w.n.	10	C	HGS	Sa/Niell

AC	SC	RC	PCV	Sh	SI	A	TGR
NMA	JPL	IGS	NGS(a)	30 min	300 s	No	Yes
NMA	IGS	IGS	NGS(a)	30 min	300 s[a]	No	Yes
ROA	JPL	IGS	NGS(r)	30 min	300 s	No	Yes
UPC	JPL	No	IGS	30 min	300 s	No	No
UPC	IGS	No	IGS	30 min	300 s[a]	No	No
UNOTT	IGS	IGS	IGS	–	900 s	No	No
UNOTT	IGS	IGS	IGS	–	900 s	No	No
SRC	IGS	IGS	IGS	–	30 s	QIF	–
GCM	IGS	IGS	IGS	–	30 s	No/f	–

The columns are: AC: analysis centre, P: program used for the analysis, S: analysis strategy, GP: global products (SOCs and EOPs), CM: clock model, γ: cut-off elevation angle, GM: geophysical models, OL: ocean loading, AMF: atmospheric mapping function, SC: satellite phase centre corrections, RC: receiver cross-correlation corrections, PCV: phase center variations, Sh: length of interval, for which observations are removed after satellite was in earth shadow, SI: sampling interval, A: ambiguity fixing, TGR: tropospheric gradients. Other abbreviations are: w.n.: 'white noise', RNS: regional network solution, C: according to IERS and IGS conventions, HGS: Scherneck, http://www.oso.chalmers.se/loading, Niell: Niell mapping function, Sa: Saastamoinen model for zenith delay, NGS: National Geodetic Service, a: absolute, r: relative f: ambiguities are removed, QIF: quasi ionosphere free. The ACs are: GCM: General Command of Mapping, Ankara, Turkey, NMA: Norwegian Mapping Authority, Norway, ROA: Real Instituto y Observatorio de la Armada, Cadiz, Spain, SRC: SRC Space Research Centre, Polish Academy of Science, Warsawa, Poland, UNOTT: Institute of Engineering Surveying and Space Geodesy, University of Nottingham, UK, UPC: Universidad Politecnica de Cataluna Barcelona, Spain.

[a] 900 s before November 5, 2000.

and assessment. In the following, we concentrate solely on the height component.

The goal of the comparison presented here is an assessment of the different solutions provided by the ACs, and should not be regarded as a coordinate time series analysis strategy trying to estimate the most accurate secular trends. For details of the time series strategy that aims to accomplish this, the reader is referred to Teferle et al. (2007).

The comparison is based on two aspects, namely (1) the cross-correlation matrix between the nine different solutions for individual stations, and (2) a time series analysis based on a least squares fit of a model function to each time series.

For each station, the standard cross-correlation matrix is computed for all available height time series after removing constant offsets and trends as well as jumps. From these individual station matrices, an average correlation matrix is derived.

In order to parametrize the time series, the model function

$$h(t) = a + bt + \sum_{j=1}^{2}\{A_j \sin \omega_j t + B_j \cos \omega_j t\} + \sum_{j=1}^{n} C_j H(t - T_j) \quad (1)$$

is used, where h is the height value, t the time, ω_1 and ω_2 the angular frequency of an annual and semi-annual harmonic constituent, and A_j and B_j their respective amplitudes of the sine and cosine parts. The coefficients C_j are the magnitude of offsets described by the Heaviside function

$$H(t) = \{0\ t < 0, 1\ t \geqq 0\} \quad (2)$$

and the time of the offset T_j. n is the number of jumps included.

In the least squares fit of Eq. (1) to the individual time series, we solved for the offset a, the rate b, the coefficients A_j and B_j of the annual and semi-annual harmonic constituents. Moreover, we solved for the magnitude C_j of obvious jumps in the time series identified either from log-file information or visually in the time series.

At 2001-12-02, IGS made a transition from IGS97 to IGS00, such that IGS precise SOCs given in IGS97 need to be transformed in order to be combinable with the SOCs provided after the transition date. However, the transformation from IGS97 to IGS00 provided by IGS did not remove all of the effect, leaving an apparent offset in height of 6–10 mm for stations in Europe, due to the fact that IGS precise orbits are given in a specific frame that is not identical to IGS00 (for details see Kierulf et al. (2004)). Clearly, not solving for this offset would result in a biased trend estimate of between 3 and 5 mm/yr, for a time span of four years. To get comparable time series, offsets are also included in the time series not affected by the reference

frame transition. The effect on the results is generally much smaller than the differences between the different strategies.

4. Results

In Figs. 2 and 3, the nine different time series provided by the six ACs are shown for the stations HELG and NSTG, respectively. These two stations constitute the end points in terms of quality: HELG, at the high end, is a high-quality station without any gaps and offsets, while NSTG, at the low end, exhibits a number of gaps and offsets. Moreover, the latter station is affected by radio frequency interference and multipath (Teferle et al., 2003).

Unfortunately, very recently an error was discovered in the Bernese software (Fridez, 2004). This error can cause periodic variations of the order of 1 cm in regional networks. Therefore, we have excluded the time series from UNOTT and SRC from most of the further discussion.

The cross-correlation matrices for these two stations (Tables 3 and 4) as well as the means of the cross-correlations (Table 5) indicate large differences in the day-to-day variations obtained for the different solutions. In general, the cross-correlation coefficients ρ_{ij}, where i and j indicate the two solutions in a pair, are lower for NSTG than for HELG, which may be a result of different handling of data of poor quality in the different software packages. Turning to the average values for ρ_{ij}, the highest value is found for the NMA-JPL and ROA solutions, which is not surprising, since the two solutions are identical in almost all parameters listed in Table 2. Thus, the still considerable deviation

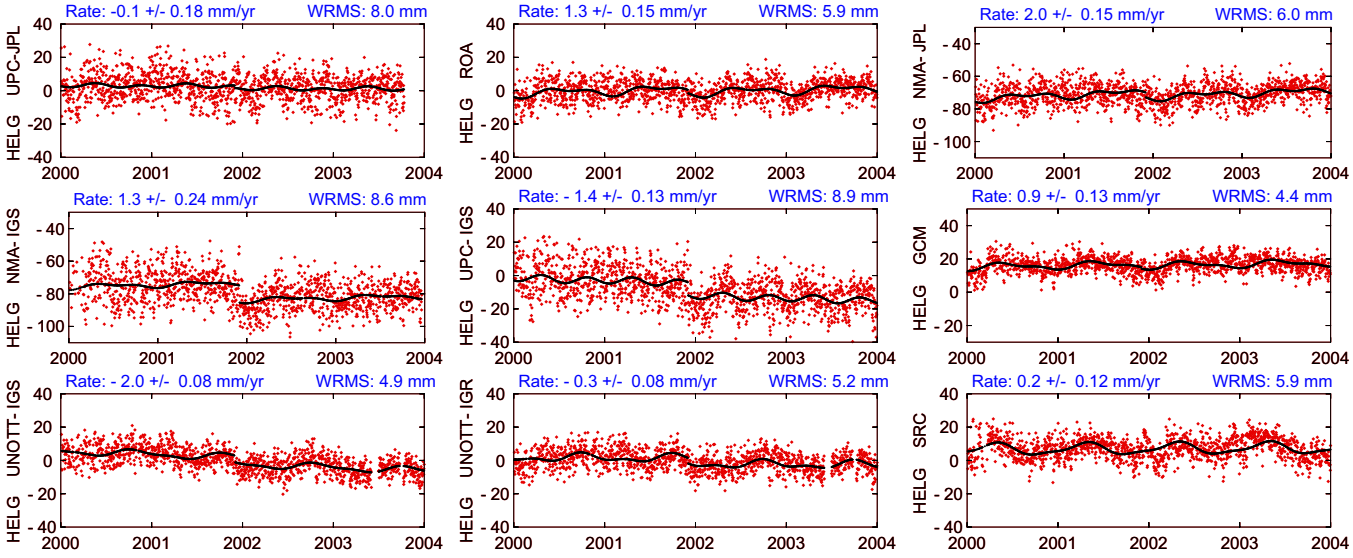

Fig. 2. Time series of vertical displacements for HELG. For the ACs see Table 2. Time is in years and displacements are in millimeters.

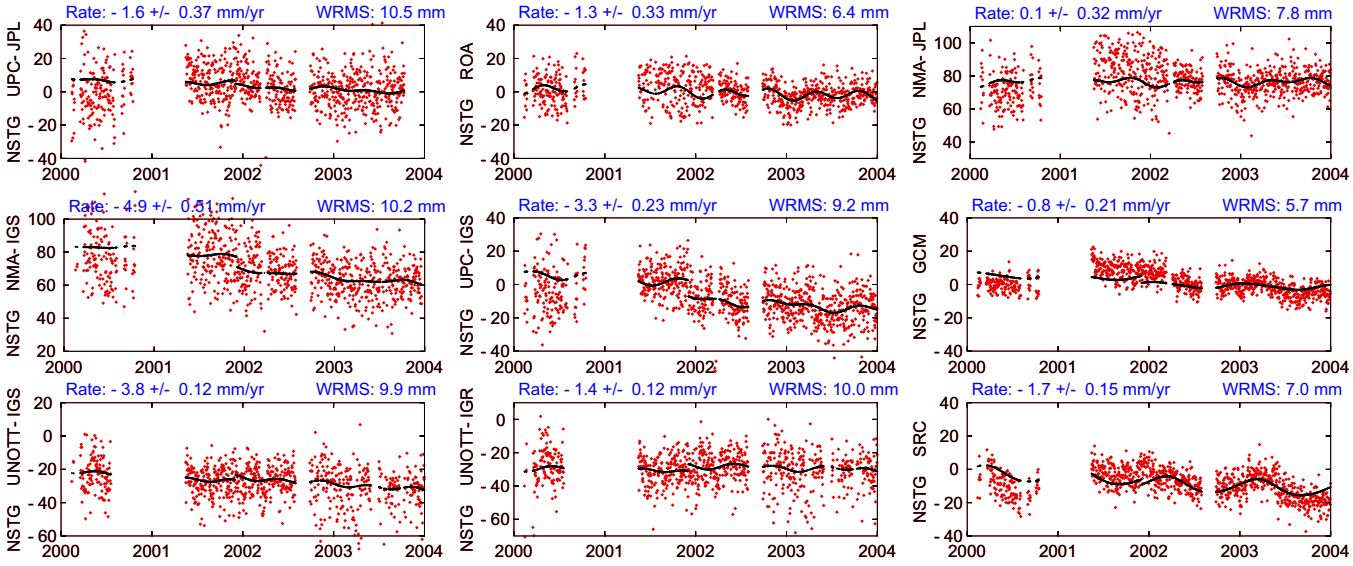

Fig. 3. Time series of vertical displacements for NSTG. For the ACs see Table 2. Time is in years and displacements are in millimeters.

Table 3
Covariance for HELG

HELG	NMA-JPL	ROA	UPC-JPL	NMA-IGS	UPC-IGS	GCM	SRC	UNOTT-IGS	UNOTT-IGR
NMA-JPL	1.00	0.94	0.66	0.42	0.39	0.49	0.29	0.33	0.32
ROA	0.94	1.00	0.67	0.41	0.39	0.52	0.31	0.33	0.33
UPC-JPL	0.66	0.67	1.00	0.34	0.49	0.52	0.33	0.33	0.32
NMA-IGS	0.42	0.41	0.34	1.00	0.72	0.41	0.27	0.29	0.26
UPC-IGS	0.39	0.39	0.49	0.72	1.00	0.45	0.31	0.26	0.24
GCM	0.49	0.52	0.52	0.41	0.45	1.00	0.56	0.33	0.35
SRC	0.29	0.31	0.33	0.27	0.31	0.56	1.00	0.16	0.17
UNOTT-IGS	0.33	0.33	0.33	0.29	0.26	0.33	0.16	1.00	0.79
UNOTT-IGR	0.32	0.33	0.32	0.26	0.24	0.35	0.17	0.79	1.00

Table 4
Covariance for NSTG

NSTG	NMA-JPL	ROA	UPC-JPL	NMA-IGS	UPC-IGS	GCM	SRC	UNOTT-IGS	UNOTT-IGR
NMA-JPL	1.00	0.86	0.37	0.36	0.21	0.35	0.21	0.04	0.03
ROA	0.86	1.00	0.41	0.34	0.24	0.26	0.16	0.07	0.06
UPC-JPL	0.37	0.41	1.00	0.21	0.53	0.34	0.29	0.14	0.13
NMA-IGS	0.36	0.34	0.21	1.00	0.47	0.19	0.12	0.12	0.11
UPC-IGS	0.21	0.24	0.53	0.47	1.00	0.36	0.24	0.11	0.10
GCM	0.35	0.26	0.34	0.19	0.36	1.00	0.55	0.09	0.09
SRC	0.21	0.16	0.29	0.12	0.24	0.55	1.00	0.05	0.05
UNOTT-IGS	0.04	0.07	0.14	0.12	0.11	0.09	0.05	1.00	0.83
UNOTT-IGR	0.03	0.06	0.13	0.11	0.10	0.09	0.05	0.83	1.00

of these ρ-values from the expected value of 1.0 are mainly explained by the difference in the use of absolute versus relative receiver antenna phase centre values (see http://www.ngs.noaa.gov/ANTCAL/images/ant_info.html). Furthermore, the analyses with GIPSY could also be influenced by some hidden factors, which are handled differently by the two ACs. Using IGS SOCs instead of the JPL SOCs produces significantly different time series, and ρ for NMA-JPL and NMA-IGS is as low as 0.4. The main differences between the UPC solution on the one side and the NMA and ROA solutions on the other side are the lower cut-off elevation used by UPC and a different treatment of the troposphere, where NMA and ROA include gradients while UPC does not. Obviously, these differences in the analysis significantly change the temporal characteristics of the solution.

Taking into account that the Bernese solutions are affected by the error in the software, we can still point out a few characteristics. The SRC solution uses only one reference station at Wettzell (WTZR) to link the solution to ITRF2000. Therefore, the time series are strongly affected by any motion of that station. As a consequence, the SRC solutions are uncorrelated with the other solutions.

For the UNOTT solutions, the regional filtering technique was applied to remove a daily common systematic bias from the coordinate time series (Wdowinski et al., 1997; Nikolaidis, 2002). On the one hand, regional filtering improves the signal-to-noise ratio in coordinate time series for stations in a regional network, but, on the other hand, decouples the filtered solutions from the global reference frame required for sea level studies. Consequently, the cross-correlation between the UNOTT solutions and any of the other solutions is not significant. Exchanging IGS precise SOCs against IGS rapid SOCs in the UNOTT solution also affects the time series, though to a much lesser extent than expected. Cross-correlation between the GIPSY solutions on the one side and the Bernese and GAMIT solutions on the other side are generally below 0.4 and the SRC solutions are nearly uncorrelated with the other solutions.

The cross-correlation clearly reveals that the temporal characteristics of the time series strongly depends on the combination of SOCs, programs, reference fixing, and last, but maybe not least, the AC. A remaining question is how much of the differences in the day-to-day variations can be attributed to variations in the reference frame implicitly used and how much has to be attributed to varying influence of noise.

Turning to the difference in estimated secular rates for the different NSTG time series we see a large spread from −4.9 mm/yr to 0.1 mm/yr. This may again be taken as an indication that the different analyses respond differently to data problems. However, also the time series for HELG result in different trend estimates ranging from −2.0 mm/yr to 2.0 mm/yr.

To examine if the length of the time series could explain the large and systematical differences between the time series, convergence plots were created for all stations. Data for the last 1.5, 2, 2.5, 3, 3.5 and 4 years before 2004 are used. For the good stations the rates for each analysis centre converge for all time series longer than 2.5 year,

Table 5
Mean corariance for ESEAS ACs

LIVE	NMA-JPL	ROA	UPC-JPL	NMA-IGS	UPC-IGS	GCM	SRC	UNOTT-IGS	UNOTT-IGR
NMA-JPL	–	0.90 ± 0.05	0.57 ± 0.13	0.39 ± 0.07	0.31 ± 0.08	0.36 ± 0.08	0.19 ± 0.06	0.23 ± 0.08	0.22 ± 0.08
ROA	0.90 ± 0.05	–	0.61 ± 0.13	0.39 ± 0.08	0.33 ± 0.07	0.38 ± 0.10	0.18 ± 0.07	0.24 ± 0.08	0.24 ± 0.07
UPC-JPL	0.57 ± 0.13	0.61 ± 0.13	–	0.26 ± 0.08	0.46 ± 0.09	0.37 ± 0.11	0.20 ± 0.11	0.23 ± 0.09	0.23 ± 0.09
NMA-IGS	0.39 ± 0.07	0.39 ± 0.08	0.26 ± 0.08	–	0.67 ± 0.12	0.24 ± 0.10	0.10 ± 0.07	0.16 ± 0.12	0.15 ± 0.12
UPC-IGS	0.31 ± 0.08	0.33 ± 0.07	0.46 ± 0.09	0.67 ± 0.12	–	0.32 ± 0.16	0.16 ± 0.11	0.15 ± 0.09	0.14 ± 0.07
GCM	0.36 ± 0.08	0.38 ± 0.10	0.37 ± 0.11	0.24 ± 0.10	0.32 ± 0.16	–	0.36 ± 0.10	0.27 ± 0.09	0.27 ± 0.09
SRC	0.19 ± 0.06	0.18 ± 0.07	0.20 ± 0.11	0.10 ± 0.07	0.16 ± 0.11	0.36 ± 0.10	–	0.21 ± 0.13	0.23 ± 0.13
UNOTT-IGS	0.23 ± 0.08	0.24 ± 0.08	0.23 ± 0.09	0.16 ± 0.12	0.15 ± 0.09	0.27 ± 0.09	0.21 ± 0.13	–	0.83 ± 0.05
UNOTT-IGR	0.22 ± 0.08	0.24 ± 0.07	0.23 ± 0.09	0.15 ± 0.12	0.14 ± 0.07	0.27 ± 0.09	0.23 ± 0.13	0.83 ± 0.05	–

confirming that 2.5 years of data is enough to determine rates at a reasonable level if periodic signals are resolved (see Blewitt and Lavallée, 2002). However, the systematical differences between the ACs remain and demonstrate that the rate differences are mainly caused by the different reference frame realisations and that the time series approach sufficient lengths. In Fig. 4 the convergence plot for HELG is shown. For the problematic station NSTG, the picture is not so clear (Fig. 5). This is not surprising taking into account that this station is heavily influenced by discontinuities and bad data.

Table 6 gives the results for the 13 stations, which are those considered to be of a high quality. In order to allow for a separation of the seasonal cycle from secular trends, only records covering more than three years (Table 1) are included in the comparison. To avoid problems related to resolving jumps, only stations where the antenna and receiver are unchanged during the actual period, are regarded. Furthermore, the stations ACOR, MORP and NSTG are

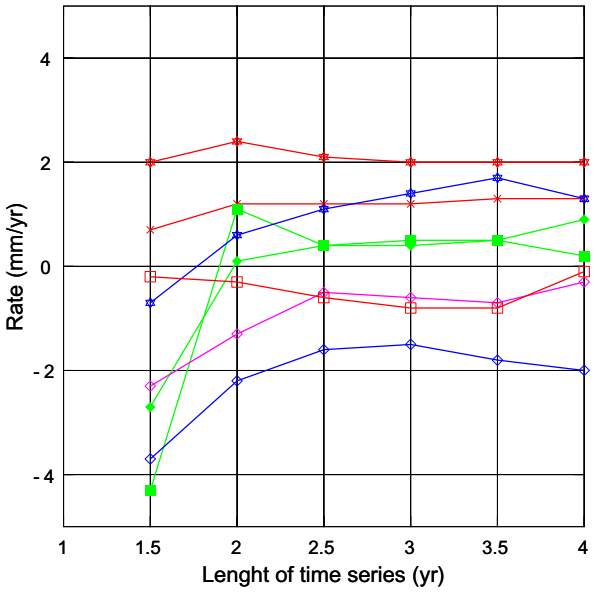

Fig. 4. Convergence plot HELG. The symbols represent the ACs: NMA-star, ROA-times, UPC-box, SRC-filled box, UNOTT-diamond and GCM-filled diamond. The colours represent the strategy and SOC combination: JPL(PPP)-red, IGS(PPP)-blue, IGR(PPP)-violet and IGS(DD)-green. (For interpretation of the references to colour in this figure legend, the reader is referred to the web version of this article.)

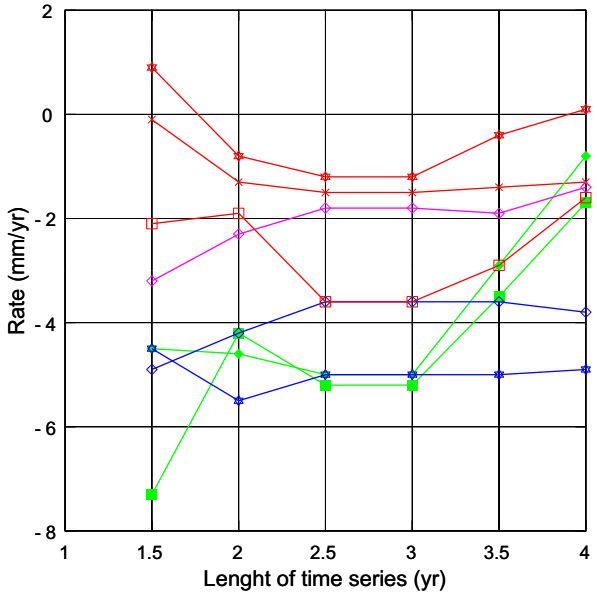

Fig. 5. Convergence plot NSTG. The symbols represent the ACs: NMA-star, ROA-times, UPC-box, SRC-filled box, UNOTT-diamond and GCM-filled diamond. The colours represent the strategy and SOC combination: JPL(PPP)-red, IGS(PPP)-blue, IGR(PPP)-violet and IGS(DD)-green. (For interpretation of the references to colour in this figure legend, the reader is referred to the web version of this article.)

encumbered with data gaps and poor data quality and were consequently excluded. For most stations, the spread of trends is similar to the one found for HELG. The mean values of the trends cluster in three groups, namely those for (1) the GIPSY and JPL SOC combinations, (2) the regionally filtered UNOTT solutions, and (3) the other solutions using IGS SOCs.

In group 1, the trends for ROA and NMA-JPL for single stations show deviations of the order of ±1 mm/yr, which is large taking into account that the analyses are carried out with almost identical parameters (see Table 2). The only difference is the use of absolute versus relative receiver antenna phase centre values. The trends for UPC-JPL agree with the ROA and NMA-JPL series reasonably well for two stations, but differ for HELG and even more so for CASC. The reason for the large difference for CASC is not known. However, UPCs strategy differs mainly in two ways, by the use of a lower cut-off elevation than ROA

Table 6
Rates for CGPS time series of vertical displacements

AC SOC STAT	NMA-JPL (mm/yr)	ROA-JPL (mm/yr)	UPC-JPL (mm/yr)	NMA-IGS (mm/yr)	UPC-IGS (mm/yr)	GCM-IGS (mm/yr)	SRC-GS (mm/yr)	UNOTT-IGS (mm/yr)	UNOTT-IGR (mm/yr)	Mean**	Median** min/max (mm/yr)
ABER	0.9	−0.1	0.2	−0.3	−1.1	−1.5	−2.0	−6.1	−3.7	−0.6± 0.9	−2.0 < −0.3 < 0.9
ALAC	0.9	0.1	–	0.6	–	−0.8	0.4	−3.0	−2.4	0.2 ± 0.6	−0.8 < 0.4 < 0.9
ANDO	0.0	0.4	−0.5	−1.9	−3.3	−1.0	1.1	−7.0	−5.1	−0.7± 1.4	−3.3 < −0.5 < 1.1
CAMB	0.3	0.7	–	−0.3	–	−1.0	−0.5	−3.4	−2.0	−0.2 ± 0.6	−1.0 < −0.3 < 0.7
CASC	−0.5	0.1	4.1	0.2	3.4	−1.6	−0.3	−2.4	−0.6	0.8 ± 2.0	−1.6 < 0.1 < 4.1
GENO	−1.7	−0.6	–	0.3	–	−1.9	−1.7	−3.7	−1.8	−1.1 ± 0.8	−1.9 < −1.7 < 0.3
HELG	2.0	1.3	−0.1	1.3	−1.4	0.9	0.2	−2.0	−0.3	0.6 ± 1.0	−1.4 < 0.9 < 2.0
LIVE	1.3	1.1	–	−1.0	–	−0.3	2.4	−3.5	−1.2	0.7 ± 1.2	−1.0 < 1.1 < 2.4
LOWE	1.1	1.0	–	−0.6	–	−0.5	2.5	−3.7	−1.7	0.7 ± 1.2	−0.6 < 1.0 < 2.5
NEWL	0.9	1.4	–	0.7	–	−0.3	−0.4	−2.7	−1.0	0.5 ± 0.7	−0.4 < 0.7 < 1.4
NYA1	6.1	6.2	–	4.8	–	–	–	–	–	5.7± 0.6	4.8 < 6.1 < 6.2
NYAL	6.0	6.2	–	4.6	–	–	–	–	–	5.6± 0.7	4.6 < 6.0 < 6.2
SHEE	1.6	0.4	–	0.0	–	0.0	−1.2	−4.2	−1.9	0.2 ± 0.9	-1.2 < 0.0 < 1.6
Mean*	0.6	0.5	0.9	−0.1	−0.6	−0.7	0.0	−3.8	−2.0		
Relative	0.0± 0.0	−0.1± 0.7	0.3± 2.5	−0.8± 1.1	−1.2± 3.0	−1.3± 0.5	−0.6± 1.4	−4.4± 1.6	−2.6± 1.5		

The rates are from the least squares fit of Eq. (1) to the different solutions provided by the ESEAS ACs.
Mean* is the mean of all stations except NYAL and NYA1.
Mean** and Median** are based on all ACs except the two UNOTT solutions.
Relative is the mean of all stations relative to the NMA-JPL solution.

and NMA-JPL, and by not estimating tropospheric gradients. Different cut-off elevations influence the vertical trend and the effect may be as large as several mm/yr (Kierulf et al., 2001). Moreover, taking into account tropospheric gradients has an effect on intra-seasonal and seasonal variations and thus on the temporal characteristics of the time series. It may also affect the trends in a minor way.

The trends for the UNOTT solutions are on average much lower than those for groups 1 and 3, which can be attributed to a combination of the reference frames of the IGS and IGR SOCs and the current CGPS processing strategy, and additionally to the regional filtering. It can be shown that the magnitude of the reference frame and strategy related effect on the trends is on average at the several mm/yr level, whereas the effect stemming from the filtering accounts for only about 0.5 mm/yr. The mean trends for group 1 are approximately 1.0 mm/yr greater than those of group 3.

Using the weighted Root Mean Square (RMS) values from the least squares fit of Eq. (1) to the time series as an indication of the quality of the time series (Table 7), we note that for the PPP results, GIPSY achieves lower RMS values when used with JPL SOCs than with IGS precise SOCs. The daily geocentre motion (up to 1 cm) maps into IGS SOCs (Kouba and Springer, 2001; Ray et al., 2004) and this may to a large extent explaine the latter. In addition could the close connection between GIPSY and JPL SOCs contribute to an reduced RMS for the GIPSY solutions using JPL SOCs. The same software with exactly the same geophysical models and parameters are used both in the SOC determination and in the PPP analysis. Moreover, the IGS SOCs are products combined from individual solutions using different software packages and analysis strategies. Consequently, the PPP analysis based on IGS SOCs is inconsistent with the SOC determination. For the DD solutions, the Gamit-DD solutions have lower RMS values than the Bernese-DD solutions for almost all stations. In addition to the potential effect of the error in the Bernese software, this can be explained by the difference in reference frame fixing applied by GCM and SRC, respectively.

Finally, we present the amplitudes and phase of the annual constituent as determined in the fit of Eq. (1) to the time series (Tables 8), excluding, however, the Bernese solutions. For the presumably identical analyses of NMA-JPL and ROA, the difference in amplitude and phase are in general not significant. The NMA-IGS solutions show considerable differences in amplitude and phase compared to the NMA-JPL results, which are attributed to different seasonal variations of the origin of the two reference frames for these solutions. Similarly, large differences are found between UPC-JPL and UPC-IGS.

For most stations RMS values are on the level of what can be expected for vertical coordinate time series in a global reference frame. This is taken as an indication that all ACs carry out analyses with high precision, not neglecting the fact that the results of two ACs are compromised by a

Table 7
RMS for the CGPS time series of vertical displacements

AC SOC STAT	NMA-JPL (mm)	ROA-JPL (mm)	UPC-JPL (mm)	NMA-IGS (mm)	UPC-IGS (mm)	GCM-IGS (mm)	SRC-IGS (mm)	UNOTT-IGS (mm)	UNOTT-IGR (mm)
ABER	5.9	5.5	7.4	7.8	8.1	3.9	6.6	6.0	6.3
ALAC	6.3	6.1	–	9.3	–	4.9	7.3	5.5	5.6
ANDO	8.0	6.4	7.7	8.9	9.0	4.7	8.7	7.2	7.8
CAMB	6.2	5.7	–	8.5	–	4.3	8.8	6.1	6.1
CASC	5.9	5.8	7.3	9.3	9.3	6.0	8.7	6.5	6.6
GENO	8.0	7.3	–	10.4	–	3.9	5.1	6.3	6.0
HELG	6.0	5.9	8.0	8.6	8.9	4.4	5.9	4.9	5.2
LIVE	6.1	5.6	–	7.7	–	3.7	6.2	5.5	5.7
LOWE	6.3	5.8	–	8.1	–	4.0	6.5	6.3	6.2
NEWL	6.3	6.0	–	8.2	–	5.4	9.0	6.9	6.8
NYA1	7.1	7.0	–	9.9	–	–	–	–	–
NYAL	7.5	7.4	–	10.4	–	–	–	–	–
SHEE	7.2	6.9	–	10.5	–	4.3	8.3	6.8	7.1

RMSs are from the least squares fit of Eq. (1) to the different solutions provided by the ESEAS ACs.

Table 8
Annual signal in the vertical displacements

AC STAT	NMA-JPL		ROA		UPC-JPL		NMA-IGS		UPC-IGS		GCM	
	Amp. (mm)	Pha. (d)	Amp. (mm)	Pha. (d)	Amp. (mm)	Pha. (d)	Amp. (mm)	Pha. (d)	Amp. (mm)	Pha. (d)	Amp. (mm)	Pha. (d)
ABER	0.4	–131.9	0.5	129.5	1.2	45.3	0.6	-60.3	1.3	40.5	1.7	64.0
ALAC	1.5	140.8	1.5	140.2	–	–	1.3	154.2	–	–	2.7	42.3
ANDO	3.4	−104.4	2.4	−111.1	1.4	−57.7	3.8	−52.7	2.6	−47.7	1.0	−156.9
CAMB	0.8	77.6	1.3	79.9	–	–	1.8	90.9	–	–	2.8	78.2
CASC	0.4	−152.9	0.5	−159.2	0.6	165.3	1.2	−107.4	0.7	−142.2	4.4	23.9
GENO	2.2	−141.2	1.7	−124.5	–	–	1.0	−121.1	–	–	0.9	−101.9
HELG	1.6	−151.7	2.0	−158.9	0.6	134.3	1.2	160.8	0.4	73.9	1.8	151.9
LIVE	1.2	−3.0	1.0	7.0	–	–	1.0	6.5	–	–	1.8	39.0
LOWE	0.5	−166.3	0.1	−151.4	–	–	0.4	78.4	–	–	1.2	69.4
NEWL	1.0	−160.4	0.6	120.2	–	–	0.5	70.8	–	–	2.0	73.9
NYA1	3.4	−61.3	3.4	−60.5	–	–	6.0	−50.9	–	–	–	–
NYAL	3.6	−60.8	3.6	−58.4	–	–	6.7	−52.6	–	–	–	–
SHEE	2.4	−144.3	2.8	−143.5	–	–	1.6	−167.0	–	–	1.9	−178.8

Amplitudes (Amp.) and phases (Pha.) are determined in the least squares fit of Eq. (1) to the different solutions provided by the ESEAS ACs.

software error. However, not only the computed rates (Table 6) but also the annual harmonic constituents (Tables 8) demonstrate large and systematic differences. The possible reasons for these differences are discussed in the next section.

5. Discussion

To study the possible reasons for the observed systematic differences in trends and harmonic constituents identified in the previous section, we will again focus on those stations that we consider to be of high quality. In Fig. 6 the difference between the individual rates and the NMA-JPL trends are plotted for each station. For most stations, the systematic deviations between the solutions as discussed above on the basis of the means are reproduced. The GIPSY-JPL solutions mostly have the highest values, while the GIPSY-IGS solutions are systematically lower. This difference between JPL and IGS based GIPSY solutions appears to depend on the latitude, with the largest differences occuring in northern areas. This pattern is in agreement with a differential motion of the origins of the frames determined by the JPL SOCs and the IGS SOCs. While the JPL-SOCs are aligned to ITRF2000 using the same origin as ITRF2000, the IGS precise SOCs use the centre of mass of the Earth system as sensed by the GPS alone as origin. The relative motion of these two origins is of the order of 2–3 mm/yr and thus sufficient to explain the differences in local trends visible in Fig. 6. Thus, this difference is due to a known difference in the reference frames (see Fig. 7).

The reference frame of the DD solutions is a regional approximation to ITRF2000. The unconstrained SINEX solutions obtained with the GAMIT software are constrained to ITRF2000 using nine selected IGS stations. Thus, this solution is affected by any difference in the geocentric motion of the regional reference network with respect to ITRF2000. Such differential motion can only be detected from either a PPP analysis of the reference stations or a global analysis including the reference stations.

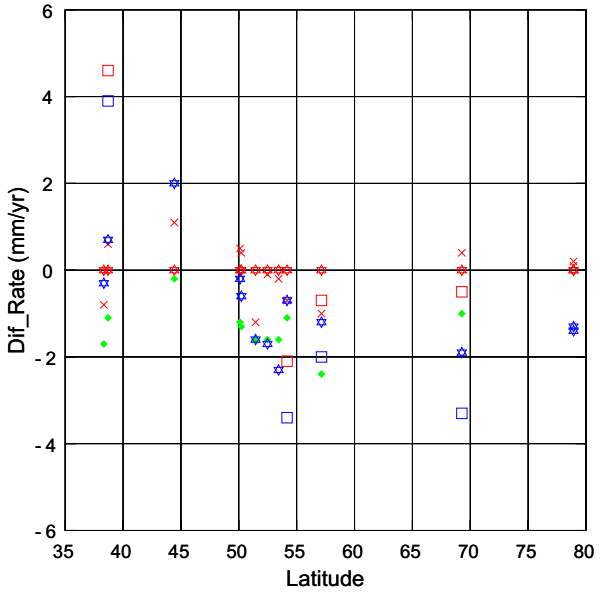

Fig. 6. Vertical trends at the CGPS sites. The rates are given relative to the NMA-JPL solutions and are plotted as function of latitude of the station. The symbols represent the ACs: NMA-star, ROA-times, UPC-box, and GCM-filled diamond. The colours represent the strategy and SOC combination: JPL(PPP)-red, IGS(PPP)-blue, and IGS(DD)-green. (For interpretation of the references to colour in this figure legend, the reader is referred to the web version of this article.)

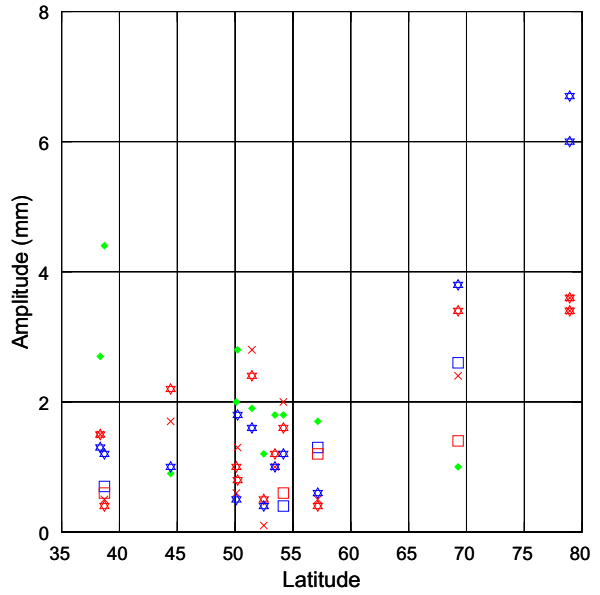

Fig. 7. Annual signal in vertical displacements. The amplitudes are plotted as function of the latitude of the station. The symbols represent the ACs: NMA-star, ROA-times, UPC-box, and GCM-filled diamond. The colours represent the strategy and SOC combination: JPL(PPP)-red, IGS(PPP)-blue, and IGS(DD)-green. (For interpretation of the references to colour in this figure legend, the reader is referred to the web version of this article.)

In the third group, the UPC-IGS (GIPSY) solutions deviate most from the other solutions. For three of the four stations processed by this AC, the trends are significantly lower, while the trend for CASC is much higher than for the comparable analyses. The reason for that is currently not clear. However, the UPC solutions have lower cut-off elevations and different treatment of the troposphere, and particularly a different cut-off elevation may affect different stations differently, depending on the particular horizon at the site. Excluding the UPC-IGS solutions, the overall agreement of the trends is on the order of ± 1.5 mm/yr. At least a part of this can be attributed to reference frame differences, but a substantial part may also be due to other influences on the analyses.

The annual harmonic signals also show large differences between the different solutions. There is very good agreement between the ROA and NMA-JPL solution, both in amplitude and phase. Using IGS SOC in GIPSY PPP results in a completely different annual constituent, most likely due to seasonal geocenter motion treated differently in the IGS SOC and JPL SOC frames.

Considering the amplitude of the annual constituent as function of latitude, the PPP solutions exhibit a slight latitude dependence with significantly larger signal in northern areas. This dependence is most pronounced for the PPP solution with IGS products, where the amplitude for Ny-Ålesund exceeds 6 mm. The large annual signal in northern areas may partly be explained by displacements induced by loading (e.g. snow). However, that does not explain the difference between PPP-JPL and PPP-IGS. The different relations between origins of the JPL and IGS precise SOC frames and the center of mass of the Earth system can be expected to induce a latitude-dependent difference in the seasonal variation observed in the two frames.

6. Conclusions

The inter-comparison of different GPS analysis solutions reveal significant differences in the temporal characteristics of the time series. Using a complex model function for parametrization of the series, further elucidates these differences and shows that secular trends and seasonal signals to a certain extent do not represent actual vertical motion of the Earth surface with respect to the geocenter but rather artefacts of the particular analysis approaches and the differences in the reference frames.

For the GIPSY PPP analyses, the difference in the secular trends between the solutions obtained with JPL SOCs and IGS SOCs can be mostly attributed to differences in the reference frames used for the JPL and IGS SOCs. These differences can be traced back to a time-dependent translation of the two origins of the two frames with respect to each other. For global sea level studies, the crucial question is which of these two frames is better tied to the center of mass of the Earth system, and this question needs to be addressed.

Solutions based on regional alignment of the implicity reference frame to ITRF2000 turn out to be comparable to similar results obtained with the GIPSY PPP solution.

However, one has to keep in mind that regional approaches are prone to be affected by local changes at the relatively few reference stations and therefore need to be monitored very carefully. Regional filtering, which does reduce the day-to-day variations of the coordinates significantly, is found to decouple the solutions from the global reference frame and is therefore inappropriate for studies of global sea level.

Acknowledgements

All work is performed in the frame of the ESEAS-RI project, and partly funded by the European Commission under Contract EVR1-CT-2002-40025. The support of the ESEAS-RI Task 2.1 group in the development of the ESEAS Analysis strategy is acknowledged. We would thank British Isles GPS archiving Facility (BIGF), European Reference Frame (EUREF), IGS and NMA for providing access to the RINEX data for the stations. We would like to thank Etienne Orliac for his contribution to the CGPS processing at UNOTT.

References

Bevis, M., Scherer, W., Merrifield, M., (2000). Technical issues and recommendations related to the installation of continuous GPS stations at tide gauges. Available at: <http://imina.soest.hawaii.edu/cgps_tg/introduction/index.html>.

Blewitt, G., Lavallée, D., 2002. Effect of annual signals on geodetic velocities. J.Geophys. Res., 107. doi:10.1029/2001JB000570.

Church, J.A., Gregory, J.M., Huybrechts, P., Kuhn, M., Lambeck, K., Nhuan, M.T., Qin, D., Woodworth, P.L., 2001. Changes in sea level. In: Houghton, J.T., Ding, Y., Griggs, D.J., Noguer, M., van der Linden, P.J., Dai, X., Maskell, K., Johnson, C.A., (Eds.), Climate Change 2001: The Scientific Basis. Contribution of Working Group I to the Third Assessment Report of the Intergovernmental Panel on Climate Change, Cambridge University Press, Cambridge, pp. 639–694.

Fridez, P., 2004. Error number_9 [online]. Berne: The Astronomical Institute University of Berne. Available at: <http://www.bernese.unibe.ch/support.html> (Accessed 25 February 2005).

Herring, T.A., 2003. GLOBK: Globak Kalman filter VLBI and GPS Analysis Program Version 5.08. Massachusetts Institute of Technology (MIT), Cambridge.

Hugentobler, U., Schaer, S., Fridez, P., 2001. Bernese GPS Software Version 4.2. University of Berne.

Kierulf, H.P., Kristiansen, O., Plag, H.-P., 2001. Can GPS determine geocentric vertical crustal motion at the 1 mm/yr accuracy level? In: Book of Extended Abstracts, Final Workshop of COST Action 40. Hydrographic Institute of the Republic of Croatia – Split, pp. 87–91.

Kierulf, H.P., Plag, H.-P., (2004). ESEAS CGPS Processing Strategy: Determination of High Accuracy Vertical Velocities. Delivery Report D2.1 of the ESEAS-RI Project. Available at: <http://eseas.org/eseas-ri/deliverables/d2.1>, Norwegian Mapping Authority, Honefoss, Norway.

King, R.W., Bock, Y., 2003. Documentation for the GAMIT analysis software, release 10.1. Massachusetts Institute of Technology (MIT), Cambridge.

Kouba, J., 2003. A Guide to using International GPS Service (IGS) Products [online]. Pasadena: IGS Central Bureau. Available at: <http://igscb.jpl.nasa.gov/igscb/resource/pubs/GuidetoUsingIGS-Products.pdf> (Accessed 25 February 2005).

Kouba, J., Springer, T., 2001. New IGS station and satellite clock combination. GPS Solutions 4, 31–36.

Nikolaidis, R.M., 2002. Observation of geodetic and seismic deformation with the global positioning system, PhD thesis, University of California.

Ray, J., Dong, D., Altamimi, Z., 2004. IGS reference frames: status and future improvements. GPS Solutions 8 (4), 251–266.

Teferle, F.N., Bingley, R.M., Dodson, A.H., Apostoloidis, P., Staton, G., 2003. RF Interference and Multipath Effects at Continuous GPS Installations for Long-term Monitoring of Tide Gauges in UK Harbours, In: Proc. 16th Tech. Meeting of the Satellite Division of the Inst. of Navigation, ION GPS/GNSS 2003, Portland, Oregon, 9–12 September 2003, p. 12.

Teferle, F.N., Williams, S.D.P., Kierulf, H.P., Bingley, R.M., Plag, H.P., 2007. A continuous GPS coordinate time series analysis strategy for high-accuracy vertical land movements. Phys. Chem. Earth, in press, doi:10.1016/j.pce.2006.11.002.

Wdowinski, S., Bock, Y., Zhang, J., Fang, P., Genrich, J., 1997. Southern California permanent GPS geodetic array: spatial filtering of daily positions for estimating coseismic and postseismic displacements induced by the 1992 Landers Earthquake. J. Geophys. Res. 102, 18057–18070.

Zumberge, J.F., Heflin, M.B., Jefferson, D.C., Watkins, M.M., 1997. Precise point positioning for the efficient and robust analysis of GPS data from large networks. J. Geophys. Res. 102, 5005–50017.